Defect Modulation on $CaZn_{1-x}Ag_{1-y}Sb$ (0<x<1; 0<y<1) Zintl phases and Enhanced Thermoelectric Properties with High zT Plateaus

Min Zhu,[a] Zhen Wu,[a] Qian Liu,[a] Tie-Jun Zhu,[b] Xin-Bing Zhao,[b] BaiBiao Huang,[a] Xutang Tao,[a] and Sheng-Qing Xia[a]*

[a] State Key Laboratory of Crystal Materials,
Institute of Crystal Materials,
Shandong University,
Jinan, Shandong 250100, People's Republic of China
E-mail: shqxia@sdu.edu.cn

[b] State Key Laboratory of Silicon Materials
Department of Materials Science and Engineering
Zhejiang University
Hangzhou 310027, People's Republic of China

CORRESPONDING AUTHORS FOOTNOTE: Prof. Sheng-Qing Xia, State Key Laboratory of Crystal Materials, Institute of Crystal Materials, Shandong University, Jinan, ShanDong 250100; Phone: (531) 883-62519, Fax: (531) 883-62519.

Supporting Information
Contents

of suspicious impurities is indicated by a red arrow and the simulated pattern of $CaZn_{0.40(2)}Ag_{0.20(2)}Sb$ is provided for compared.

6. **Figure S4.** Plot of composition vs. lattice parameter of $CaZn_{(1-x)/2}Ag_xSb$ (x= 0.2, 0.3, 0.4, 0.5, 0.6).
7. **Figure S5.** Calculated electronic band structures of the $CaZn_{0.40(2)}Ag_{0.20(2)}Sb$. Fermi level is chosen as the energy reference.
8. **Figure S6.** TG-DSC measurements on $CaZn_{0.40(2)}Ag_{0.20(2)}Sb$, conducted in inert argon atmosphere over the temperature range of 300−1273 K.
9. **Figure S7.** Temperature dependence of the heat capacity of materials $CaZn_{1-x}Ag_{1-y}Sb$ ($0<x<1$; $0<y<1$).
10. **Figure S8.** Based on 323K Pisarenko plot of $CaZn_{(1-x)/2}Ag_xSb$ (x= 0.2, 0.3, 0.4, 0.5, 0.6) calculated with an SPB model.
11. **Figure S9.** Temperature dependence of (a) electronic thermal conductivity and (b) lattice thermal conductivity of $CaZn_{(1-x)/2}Ag_xSb$ (x= 0.2, 0.3, 0.4, 0.5, 0.6 samples.
12. **Figure S10.** Temperature dependence of power factor $S^2\sigma$ for $CaZn_{1-x}Ag_{1-y}Sb$ ($0<x<1$; $0<y<1$).
13. **Figure S11.** Based on 323K Pisarenko plot of $CaZn_{0.4}Ag_{1-y}Sb$ (y= 0.8, 0.82, 0.84, 0.86) calculated with an SPB model.
14. **Figure S12.** Temperature dependence of (a) electronic thermal conductivity and (b) lattice thermal conductivity of $CaZn_{0.4}Ag_{1-y}Sb$ (y= 0.8, 0.82, 0.84, 0.86) samples.

1. The calculation formula of Lorenz number.

For most thermoelectric materials, the actual Lorenz number depends on the reduced Fermi energy $\eta = E_f/k_BT$ and the scattering parameter r, and is determined by Eq (1), in which $F_n(\eta)$ is the Fermi integration, k_B is the Boltzmann constant, e is the electron charge, and E_f is the Fermi energy. Eq (2) shows the value of L_0 for free electrons.The reduced Fermi energy η can be derived from the Seebeck coefficient by Eq (3).

$$L = \left(\frac{k_B}{e}\right)^2 \left(\frac{(r+7/2)F_{r+5/2}(\eta)}{(r+3/2)F_{r+1/2}(\eta)} - \left[\frac{(r+5/2)F_{r+3/2}(\eta)}{(r+3/2)F_{r+1/2}(\eta)}\right]\right) \tag{1}$$

$$L_0 = \frac{\pi^2}{3}\left(\frac{k_B}{e}\right)^2 \cong 2.45\times10^{-8} W\cdot\Omega\cdot K^{-2} \tag{2}$$

$$S = \pm\frac{k_B}{e}\left(\frac{(r+5/2)F_{r+3/2}(\eta)}{(r+3/2)F_{r+1/2}(\eta)} - \eta\right) \tag{3}$$

2. EDS analysis on the single crystals of $CaZn_{0.40(2)}Ag_{0.20(2)}Sb$.

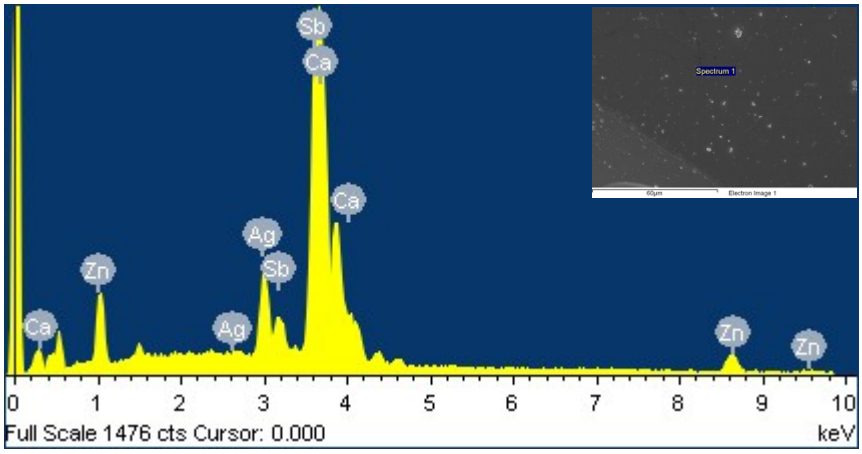

Sample 1

Element	Weight%	Atomic%	Composition
Ca K	16.36	34.41	1.00
Zn L	11.37	14.66	0.42
Ag L	10.00	7.81	0.22
Sb L	62.27	43.11	1.25

Sample 2

Element	Weight%	Atomic%	Composition
Ca K	17.51	36.17	1.00
Zn L	11.57	14.66	0.40
Ag L	10.69	8.21	0.23
Sb L	60.23	40.96	1.12

Sample 3

Element	Weight%	Atomic%	Composition
Ca K	17.69	36.36	1.00
Zn L	12.04	15.17	0.41
Ag L	10.74	8.20	0.23
Sb L	59.53	40.27	1.11

Sample 4

Element	Weight%	Atomic%	Composition
Ca K	17.88	36.80	1.00
Zn L	11.22	14.16	0.38
Ag L	11.28	8.63	0.24
Sb L	59.62	40.40	1.09

Averaged Composition: $CaZn_{0.40}Ag_{0.23}Sb_{1.17}$

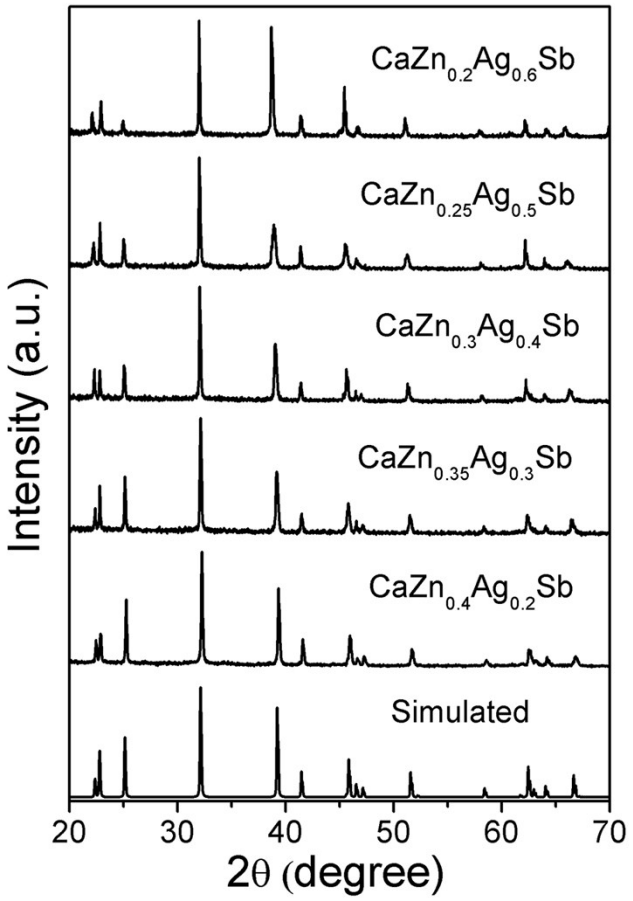

Figure S1. Powder X-ray diffraction patterns for materials with nominal compositions of $CaZn_{1-x}Ag_{1-y}Sb$ ($0<x<1$; $0<y<1$). The simulated pattern of $CaZn_{0.40(2)}Ag_{0.20(2)}Sb$ is provided for compared.

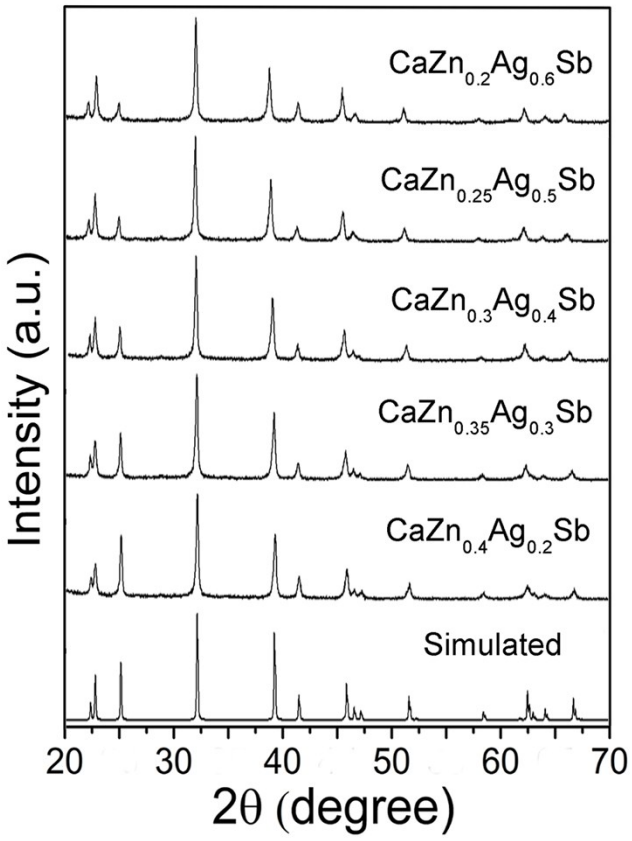

Figure S2. Powder X-ray diffraction patterns for materials with nominal compositions of $CaZn_{1-x}Ag_{1-y}Sb$ ($0<x<1$; $0<y<1$) after SPS experiments.

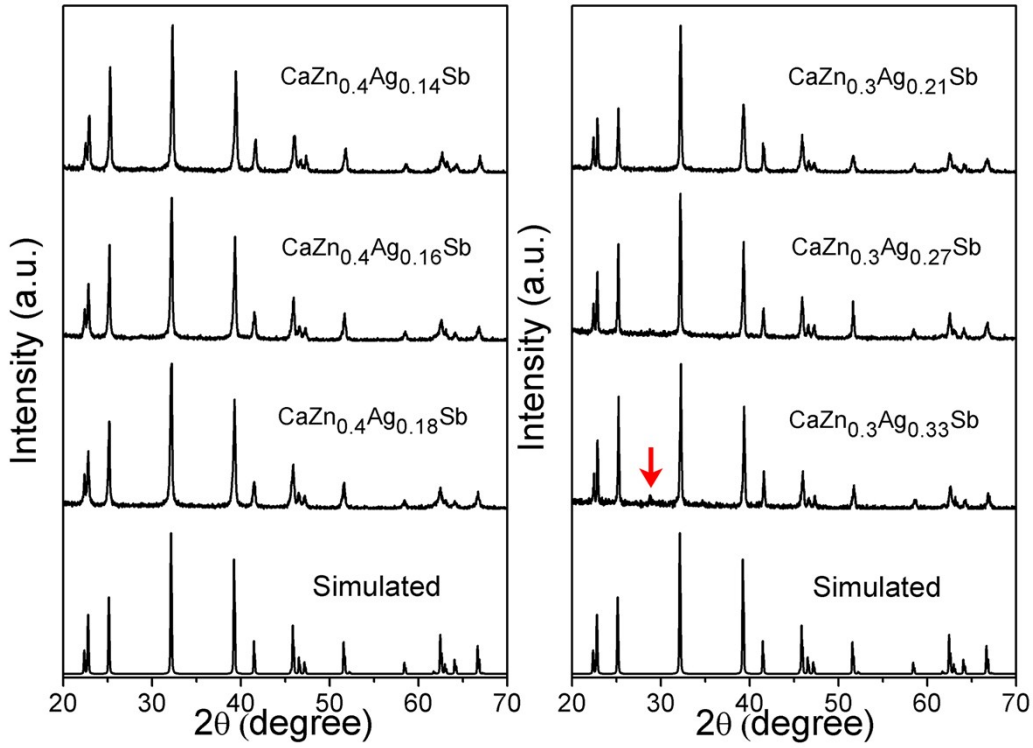

Figure S3. Powder X-ray diffraction patterns for materials with nominal compositions of $CaZn_{0.4}Ag_{1-y}Sb$ ($0<y<1$) and $CaZn_{0.3}Ag_{1-y}Sb$ ($0<y<1$). The peak of suspicious impurities is indicated by a red arrow and the simulated pattern of $CaZn_{0.40(2)}Ag_{0.20(2)}Sb$ is provided for compared.

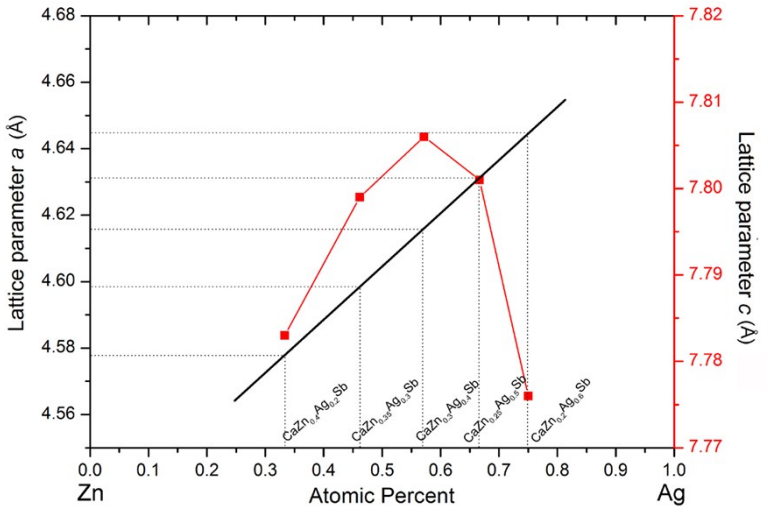

Figure S4. Plot of composition vs. lattice parameter of $CaZn_{(1-x)/2}Ag_xSb$ (x= 0.2, 0.3, 0.4, 0.5, 0.6).

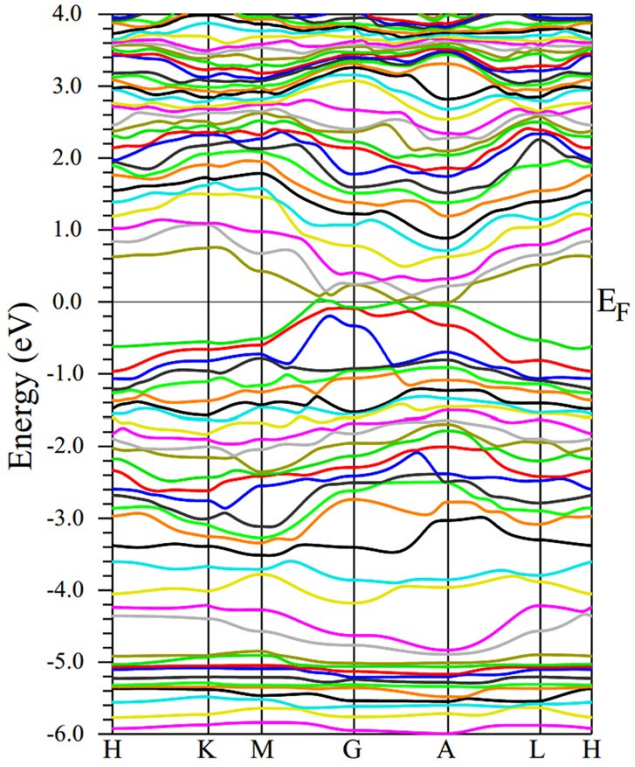

Figure S5. Calculated electronic band structures of the $CaZn_{0.40(2)}Ag_{0.20(2)}Sb$. Fermi level is chosen as the energy reference.

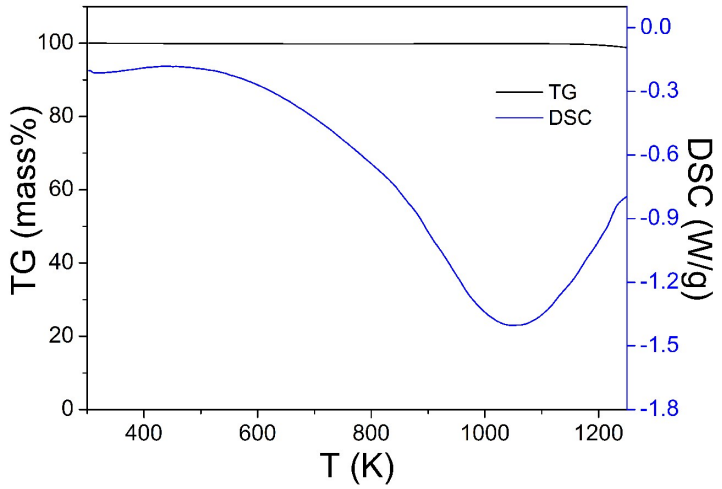

Figure S6. TG-DSC measurements on $CaZn_{0.40(2)}Ag_{0.20(2)}Sb$, conducted in inert argon atmosphere over the temperature range of 300−1273 K.

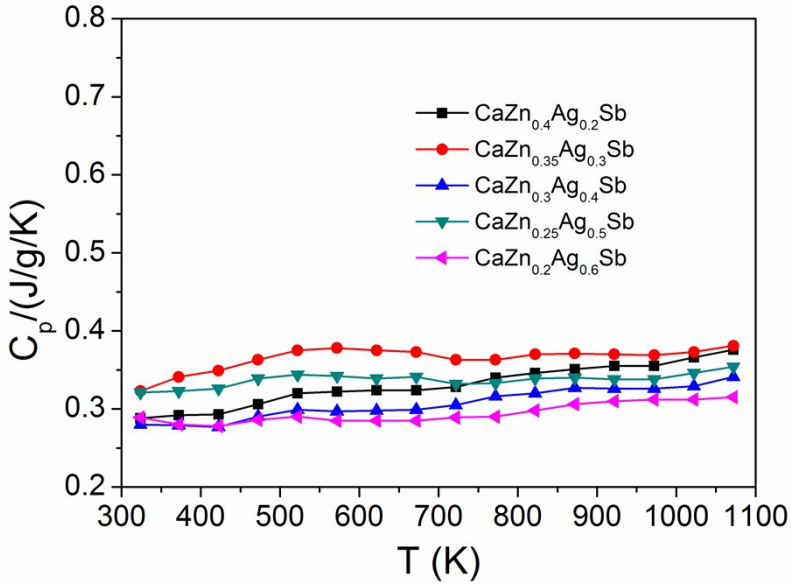

Figure S7. Temperature dependence of the heat capacity of materials $CaZn_{1-x}Ag_{1-y}Sb$ ($0<x<1$; $0<y<1$).

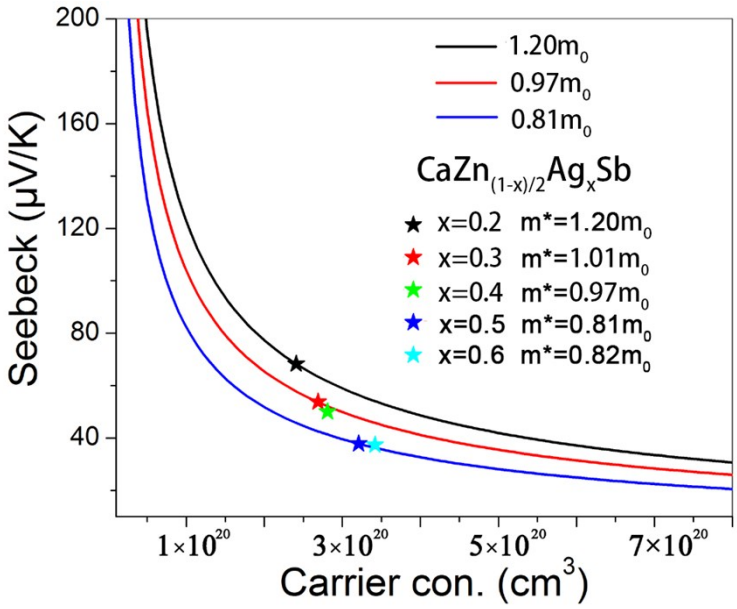

Figure S8. Based on 323K Pisarenko plot of $CaZn_{(1-x)/2}Ag_xSb$ (x= 0.2, 0.3, 0.4, 0.5, 0.6) calculated with an SPB model.

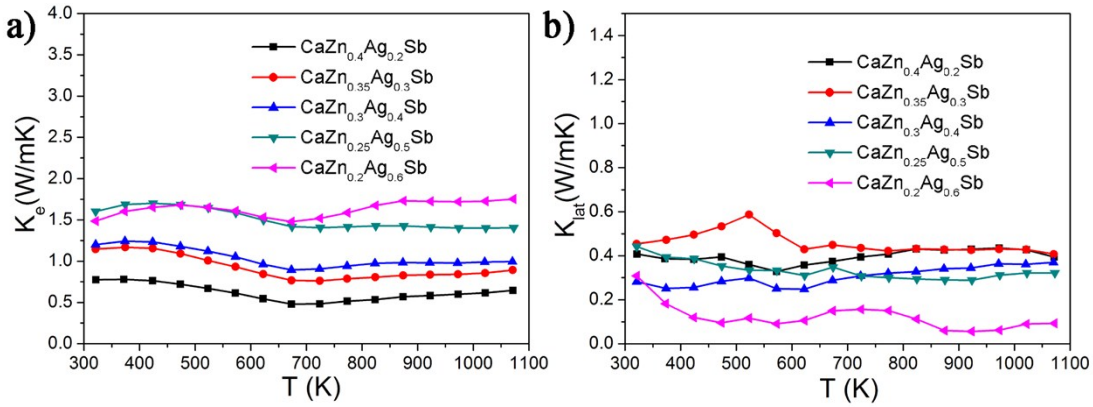

Figure S9. Temperature dependence of (a) electronic thermal conductivity and (b) lattice thermal conductivity of $CaZn_{(1-x)/2}Ag_xSb$ (x= 0.2, 0.3, 0.4, 0.5, 0.6) samples.

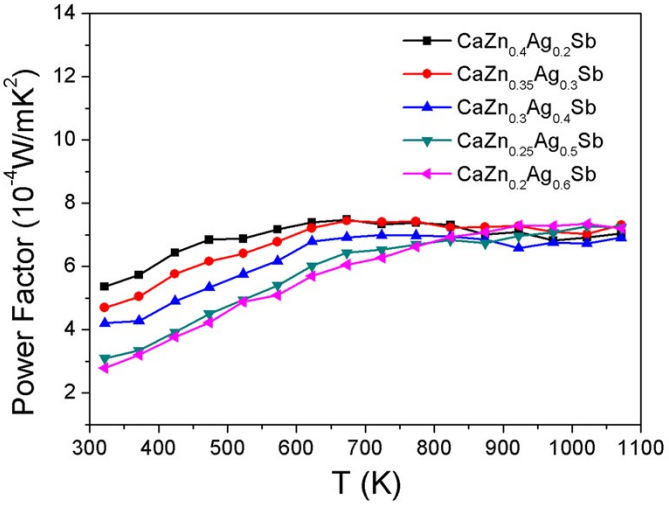

Figure S10. Temperature dependence of power factor $S^2\sigma$ for $CaZn_{1-x}Ag_{1-y}Sb$ ($0<x<1$; $0<y<1$).

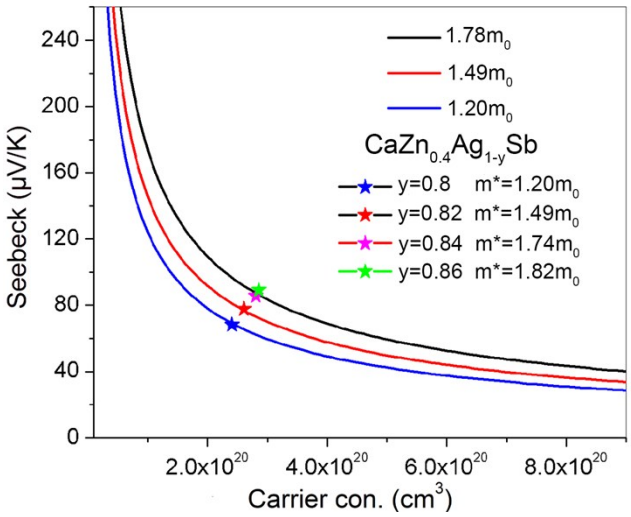

Figure S11. Based on 323K Pisarenko plot of $CaZn_{0.4}Ag_{1-y}Sb$ (y= 0.8, 0.82, 0.84, 0.86) calculated with an SPB model.

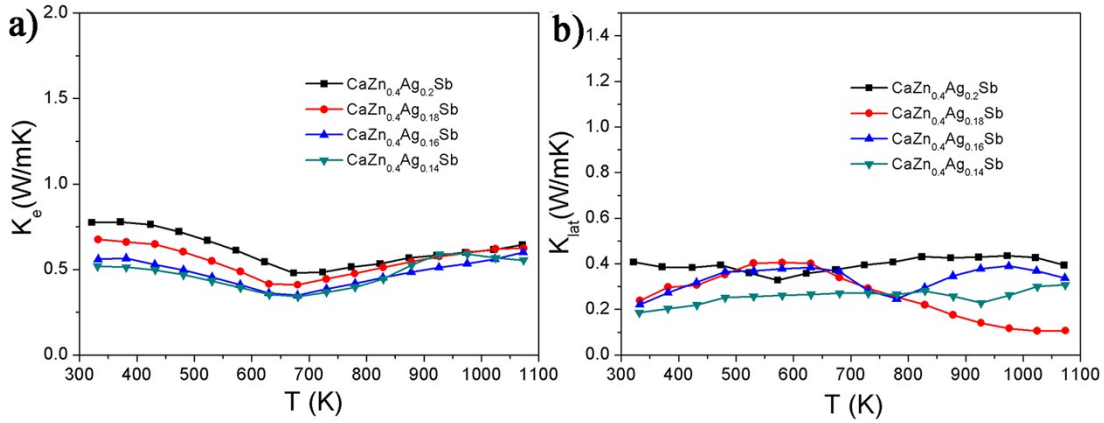

Figure S12. Temperature dependence of (a) electronic thermal conductivity and (b) lattice thermal conductivity of $CaZn_{0.4}Ag_{1-y}Sb$ (y= 0.8, 0.82, 0.84, 0.86) samples.